

PSU/TH/231
December 2000
Revised, April 2001

Expectation value analysis of wave packet solutions for the quantum bouncer: short-term classical and long-term revival behavior

M. A. Doncheski¹

Department of Physics
The Pennsylvania State University
Mont Alto, PA 17237 USA

and

R. W. Robinett²

Department of Physics
The Pennsylvania State University
University Park, PA 16802 USA

Abstract

We discuss the time development of Gaussian wave packet solutions of the ‘quantum bouncer’ (a quantum mechanical particle subject to a uniform downward force, above an impermeable flat surface). We focus on the evaluation and visualization of the expectation values and uncertainties of position and momentum variables during a single quasi-classical period as well as during the long term collapsed phase and several revivals. This approach complements existing analytic and numerical analyses of this system, as well as being useful for comparison with similar results for the harmonic oscillator and infinite well cases.

¹mad10@psu.edu

²rick@phys.psu.edu

I. Introduction

With the advent of modern computer technology, robust numerical calculations of time-dependent phenomena in quantum mechanics are now common, as is the visualization of the resulting effects [1] – [4]. The time-evolution of wave packet solutions for many scattering geometries as well as for bound state systems [5] are discussed with increasing frequency in the pedagogical literature, illustrating not only such familiar aspects as wave packet spreading, but also extending student experience to more novel phenomena such as wave packet revivals. Reviews of wave packet revivals (initially highly localized quantum wave packet solutions which exhibit quasi-classical behavior, then disperse or spread in time to a so-called collapsed phase, only to reform later to something very much like it's initial state) in many familiar model one-dimensional quantum mechanical systems such as the harmonic oscillator and infinite well have appeared [6] – [9] providing students with accessible examples of an important quantum effect which can be probed experimentally in atomic systems.

Besides studies of such effects in the two 'classic' quantum mechanical model systems mentioned above, wave packet propagation, and especially the structure of revivals, has also recently been discussed in the quantum version of another familiar classical system, the so-called quantum bouncer [10], [11]. This system is the bound state version of the classical 'falling object', and is defined by the potential energy

$$V(z) = \begin{cases} \infty & \text{for } z < 0 \\ Fz & \text{for } 0 < z \end{cases} \quad (1)$$

corresponding to a constant downwards force acting on a particle above an impenetrable flat surface at $z = 0$. Generalizing on many early papers [12] which discuss the time-independent solutions for this problem, the author of Ref. [10] focuses attention

on deriving expressions for the collapse and revival times for initially Gaussian wave packet solutions, using a mixture of numerical and analytic techniques. In this note, we will revisit this problem, along much the same lines as in Ref. [9], by examining, in detail, the short-term (quasi-classical) and long-term (revival) time-development of such solutions in terms of their position and momentum expectation values and uncertainties. This type of expectation value analysis, coupled with existing analytic, numerical, and visualization studies can then help form a more complete picture of the highly non-trivial time-development possible in one of the 'classic' one-dimensional model systems in introductory quantum mechanics.

As often happens, the more familiar and tractable cases of the harmonic oscillator and the infinite well examples exhibit special features, in this case, in terms of their time-dependence, compared to a more general form such as in Eqn. 1. For that reason, in Sec. II, we first very briefly review Gaussian wave packet solutions in these two more familiar systems. The bouncer system shares with the infinite well the feature of the 'bounce' at the impenetrable wall, but some observables, such as the time-dependent wave packet spread, exhibit a much more typical cyclic structure than for the infinite well, where only the free-particle spreading time [9] is of relevance. Since the numerical studies presented here can also make contact with analytic solutions to the problem of a particle undergoing uniform acceleration, we also mention those solutions in Sec. III and then proceed to detailed results for the quantum bouncer.

II. Gaussian wave packet solutions for the harmonic oscillator and infinite well

Because of the special nature of the energy level structure of the harmonic oscillator, any time-dependent solution of this problem, $\psi(x, t)$, will be exactly periodic and return

precisely to its initial state after the classical period, $T_{cl} = 2\pi/\omega$. Using standard propagator techniques or other methods, it is, in fact, easy to construct closed form Gaussian wave packet solutions [13] such as

$$|\psi(x, t)|^2 = \frac{1}{\sqrt{\pi}L(t)} e^{-[x-x_0 \cos(\omega t)]^2/L^2(t)} \quad (2)$$

$$|\phi(p, t)|^2 = \frac{1}{\sqrt{\pi}p_L(t)} e^{-[p+m\omega x_0 \sin(\omega t)]^2/p_L^2(t)} \quad (3)$$

which have expectation values which satisfy the classical equations of motion, namely

$$\langle x \rangle_t = x_0 \cos(\omega t) \quad \text{and} \quad \langle p \rangle_t = -m\omega x_0 \sin(\omega t). \quad (4)$$

The fact that the expectation values for any wave packet solutions for the harmonic oscillator satisfy the classical equations of motion does not depend on these specific Gaussian forms, but can be shown to be true analytically in a quite general way [14]. The solutions in Eqns. (2) and (3) have time-dependent position and momentum uncertainties given by $\Delta x_t = L(t)/\sqrt{2}$ and $\Delta p_t = p_L(t)/\sqrt{2}$ where

$$[L(t)]^2 = L^2 \cos^2(\omega t) + \left(\frac{\hbar}{m\omega L}\right)^2 \sin^2(\omega t) \quad (5)$$

$$[p_L(t)]^2 = \left(\frac{\hbar}{L}\right)^2 \cos^2(\omega t) + (Lm\omega)^2 \sin^2(\omega t) \quad (6)$$

and the parameter L sets the scale for both the position- and momentum-space spreads. Unless $L = \sqrt{\hbar/m\omega}$, these position- and momentum-uncertainties oscillate with a period twice that of the classical motion [13], regaining the initial values of Δx_0 and Δp_0 at two opposing points in phase space. Once again, these results are not specific to the Gaussian solution, but have been derived quite generally in Ref. [14]: they are also sometimes rediscovered [15], [16] in these specific cases.

Another tool which is standardly used to probe the wave packet's approximate return to the initial state is the auto-correlation function [17], defined by

$$A(t) = \int_{-\infty}^{+\infty} \psi^*(z, t) \psi(z, 0) dz = \int_{-\infty}^{+\infty} \phi^*(p, t) \phi(p, 0) dp = \sum_{n=1}^{\infty} |c_n|^2 e^{iE_n t/\hbar} \quad (7)$$

which measures the overlap of the position- or momentum-space wavefunction at later times with the initial state. For the oscillator, one can argue that because the wave packets are exactly periodic and never collapse, there are no revivals.

On the other hand, for the infinite well, because the energy levels are integral multiples of a common value (but not equally spaced), there are exact revivals [6], but initial Gaussian-type wave packets do undergo dispersion into a collapsed phase. For example, wave packets constructed from energy eigenstates via

$$\psi(x, t) = \sum_{n=0}^{\infty} c_n u_n(x) e^{-iE_n t/\hbar} \quad (8)$$

where $u_n(x) = \sin(n\pi x/L)/\sqrt{L}$ for the infinite well, with quasi-Gaussian expansion coefficients of the form

$$c_n = \sqrt{\frac{\alpha\hbar\sqrt{\pi}}{L}} e^{-\alpha^2(p_n - p_0)^2} e^{ip_n x_0/\hbar} \quad (9)$$

(where $p_n = n\hbar\pi/L$) give an initial momentum distribution very close to the standard one for Gaussian free-particle packets, namely

$$\phi_0(p) = \frac{\alpha}{\sqrt{\pi}} e^{-\alpha^2(p-p_0)^2/2} e^{ipx_0/\hbar} \quad (10)$$

and yield localized Gaussian-like position wave packets which are initially very close to the free-particle form

$$|\psi(x, t)|^2 = \frac{1}{\beta_t\sqrt{\pi}} e^{-(x-[x_0+p_0t/m])^2/\beta_t^2} \quad (11)$$

where $\beta_t = \hbar\alpha\sqrt{1+t^2/t_0^2}$ with $t_0 \equiv m\hbar\alpha^2$. Such packets undergo quasi-classical motion, bouncing back and forth between the two infinite walls, with an increasing width given roughly by an envelope defined by the time-dependent free-particle width, $\Delta x_t = \beta_t/\sqrt{2}$ [9]. During the impulsive collisions with the walls, the position-space

width temporarily decreases during the time that the momentum-space distribution is ‘flipping’ from positive to negative values.

As mentioned above, since the quantum bouncer has features in common with both systems, namely one infinite wall boundary at which ‘bounces’ will occur and a second, smoother potential barrier, we will keep both these cases in mind as we examine the short- and long-term behavior of expectation values for the quantum bouncer.

III. Expectation values for Gaussian wave packets for the quantum bouncer

Before turning to wave packet solutions of the quantum bouncer problem, we first recall some results from the related problem of a quantum particle undergoing uniform acceleration, namely subject to a constant force, F , with a potential given by $V(x) = -Fx$ everywhere in space. Transforming the resulting Schrödinger equation into momentum-space, one can construct arbitrary solutions [18] of the form

$$\phi(p, t) = \phi_0(p - Ft) e^{i[(p-Ft)^3 - p^3]/6mF\hbar} \quad (12)$$

where $\phi_0(p)$ is any initial momentum distribution. This result already implies that the momentum distribution for this case simply translates uniformly in time, with no change in shape, since

$$|\phi(p, t)|^2 = |\phi_0(p - Ft)|^2 \quad (13)$$

so that $\Delta p_t = \Delta p_0$. (We expect to see this behavior initially in the quantum bouncer case, until the wave packet nears the wall, as well as after the collision, at least for the first few classical periods.) Using this momentum-space solution, we can also construct closed-form position-space solutions; for example using the distribution

$$\phi_0(p) = \sqrt{\frac{\alpha}{\sqrt{\pi}}} e^{-\alpha^2(p-p_0)^2/2} e^{ipx_0/\hbar} \quad (14)$$

we find a general Gaussian wave packet for the accelerating particle

$$|\psi(x, t)|^2 = \frac{1}{\beta_t \sqrt{\pi}} e^{-(x - [x_0 + p_0 t/m + Ft^2/2m])^2 / \beta_t^2} \quad (15)$$

with $\beta_t = \alpha \hbar \sqrt{1 + t^2/t_0^2}$. (The same results can be obtained in a variety of ways, using operator [19] or propagator [20] methods or other techniques [21].) This solution gives

$$\langle x \rangle_t = x_0 + \frac{p_0 t}{m} + \frac{F}{2m} t^2 \quad \text{and} \quad \Delta x_t = \frac{1}{\sqrt{2}} \beta_t = \frac{\alpha \hbar}{\sqrt{2}} \sqrt{1 + t^2/t_0^2}. \quad (16)$$

Thus, the expectation value tracks the classical trajectory, while the wave packet spreads in exactly the same way as the standard free-particle Gaussian and we expect to see remnants of this behavior as well.

The author of Ref. [10] has constructed quasi-Gaussian wave packet solutions for the quantum bouncer using a combination of numerical and semi-analytic techniques, focusing on the derivation of quantities such as approximate revival time, T_{rev} . (See Ref. [6] for a very general derivation of both the classical period and quantum revival time for arbitrary bound state energy spectra). For an initial wave packet which is constructed so as to represent a particle released from rest at a height z_0 , the classical period of motion, T_{cl} , and the revival time, T_{rev} , are given by

$$T_{cl} = 2\sqrt{\frac{2mz_0}{F}} \quad \text{and} \quad T_{rev} = \frac{4}{\pi} \left(\frac{2mz_0^2}{\hbar} \right) \quad (17)$$

respectively. For simplicity, following Ref. [10], we take units such that

$$\hbar = 1, \quad 2m = 1, \quad \text{and} \quad F = 1 \quad (18)$$

and we choose particular initial values, namely

$$z_0 = 25 \quad \text{and} \quad \Delta z_0 = 1. \quad (19)$$

With these values, the classical period and revival time are given by

$$T_{cl} = 10 \quad \text{and} \quad T_{rev} = \frac{4}{\pi}(5)^2 = 795.78. \quad (20)$$

The collapse time, the time it takes for the initially localized wave packet to de-phase and become spread over the entire well, is given, in these dimensionless units as well as for our specific wavepacket parameters, as

$$T_{coll} = \frac{T_{cl}^3}{8\Delta z_0} \quad \text{or} \quad T_{coll} = 125 \quad (21)$$

respectively.

Using these parameters, we can evaluate both the position-space and momentum-space wavefunctions in a manner which is similar to that in Ref. [10]. We generate the expansion coefficients, c_n , in Eqn. (8) by explicit numerical calculation of the overlap integrals of the initial Gaussian form with the normalized energy eigenstates obtained by numerical solution of the Schrödinger equation; the eigenstates, normalization constants, and expansion coefficients are then compared to the Airy function solutions used in Ref. [10], supplemented by the more exact analytic results in Ref. [11], as a cross-check. (We truncate the expansion in eigenstates at a level consistent with the double-precision accuracy of our numerical evaluation, typically at values of the $c_n \approx 10^{-6}$; this is to be compared to the maximum values of $c_n \sim 0.5$. The resulting wavefunctions are then found to be appropriately normalized to unity to within 10^{-6} or better over all time intervals considered here.)

We use this more numerical procedure partly because this technique runs more efficiently in our computing environment, but also because we intend to eventually extend our investigations of wave packet behavior to other, more general power law potentials of the form $V_{(k)}(x) = V_0|x/a|^k$ for comparison to recent work on the revival

times in such potentials [22]. This class of potentials contains the harmonic oscillator ($k = 2$) and the infinite well ($k = \infty$) as special cases and can also be analyzed with an infinite wall added at $x = 0$ to give the quantum bouncer case (where $k = 1$): this fact also helps motivate our brief review of those two special cases.

We then plot the corresponding probability distributions over the first classical period in Fig. 1. On the left, the position-space probability is seen to spread in a manner which is numerically consistent with Eqn. (15), while the calculated position value $\langle z \rangle_t$ (solid curve) agrees well with the classical expectation for the trajectory (dashed) except, of course, for the cusp at the 'bounce'. The packet exhibits the standard 'interference' pattern during the collision with the wall [5], [23], at the 'bounce', and then reforms into something like the initial packet (compare to the dotted initial packet superimposed on the $t = 10$ case), only wider.

For the momentum-space distributions (shown on the right of Fig. 1), we also see features of both the classical motion and the uniformly accelerated wave packet. The expectation value of momentum $\langle p \rangle_t$, calculated from $|\phi(p, t)|^2$ and plotted as the solid curve, is once again consistent with the classical trajectory (dashed curve), except near the discontinuous, impulsive change in momentum values at the 'bounce'. The shape of the momentum-distribution follows the form expected from Eqn. (13), namely uniform translation with no change in shape, from $t = 1 \rightarrow t = 3$ and then again from $t = 8 \rightarrow t = 10$, that is, during the time when it is not in collision with the wall, but with a definite final change in shape, compared to the initial $|\phi_0(p)|^2$ superimposed on the $t = 10$ result. The dotted vertical lines indicate the values of $p = 0$, and also the classically expected minimum and maximum values of momentum given by $\pm p_M = \pm \sqrt{2mE} = \pm \sqrt{2mFz_0}$.

The asymmetric shape of $|\phi(p, t)|^2$ which is obvious after one period can be understood using purely classical arguments. For example, we can examine the classical

trajectories of particles released from the same height, H , but with varying initial velocities (or momenta); the resulting time-dependent momenta, $p(t)$ versus t , are shown in Fig. 2. We can see the same asymmetry arising at $t = T_{cl}$ as for the quantum mechanical $|\phi(p, t)|^2$ in Fig. 1; trajectories with momentum values $p \lesssim 0$ at $t = 0$ are shifted upwards towards $p \approx 0$ at $t = T_{cl}$, while those with $p \gtrsim 0$ are also moved to higher values to form the observed high-momentum 'tail'. (A very similar classical explanation of the time-dependent behavior of the momentum-space probability density for an otherwise free particle undergoing a 'bounce' from an infinite wall is discussed in Ref. [5]; in that case, the observed asymmetry in $|\phi(p, t)|^2$ during the 'bounce' is due to the fact that the fastest (highest momentum) components of the wavepacket strike the wall first, and hence are reversed in direction, before the slow components.)

We next focus on the time-development of quantum mechanical expectation values over the first eight classical periods and plot $\langle z \rangle_t$ and $\langle p \rangle_t$ over this interval in Fig. 3. Once again, the solid curves are the quantum mechanical expectation values, while the dashed curves are the classical trajectories. Clearly, the quantum results generally track the classical values, but become increasingly smoothed out as the packet spreads in time. We show in the same figure the time-development of the autocorrelation function, $|A(t)|^2$ versus t , over the same time interval which shows the (increasingly) approximate nature of the return to the initial state at multiples of the classical period: these results look very similar to data for wave packets in the infinite well [6], [9] as it approaches the collapsed state, while the same plot for the oscillator gives a completely periodic structure with $A(t)$ returning exactly to 1 at integral multiples of $\tau = 2\pi/\omega$.

In Fig. 4, we plot the time-dependent uncertainties in the position (Δz_t , top) and momentum (Δp_t , bottom) over the first eight classical periods. We note that the behavior of Δz_t is somewhat similar to that for the oscillator case: it initially increases

in a manner consistent with Eqn. (16) for much of the first half period, but then shrinks dramatically near $T_{cl}/2$ during the collision with the wall (as in Ref. [5]), and finally shrinks more slowly during the second half period, returning to something close to its initial spread. This behavior is different than the case of the infinite well where the wavepacket spreading is mostly determined by the free-particle expansion and more similar to the harmonic oscillator case in Eqn. (6) and general bound state systems.

In Fig. 4, the expectation value during each period is superimposed with two expressions for the spread (shown as pairs of dashed curves); specifically, for the first period we use

$$\Delta z_t = \Delta z_0 \sqrt{1 + \left(\frac{t}{t_0}\right)^2} \quad \text{and} \quad \Delta z_t = \Delta z_0 \sqrt{1 + \left(\frac{T_{cl} - t}{t_0}\right)^2} \quad (22)$$

and we extend these cyclically to later periods as shown in the figure. These agree fairly well with the observed time-dependence during the first cycle except during the collision phase, but become increasingly bad representations as the wave packet spreads into its collapsed phase. Thus, over at least the first few periods, the return to the initial spread is similar to that in Eqn. (6).

In the same figure, the spread in momentum is also illustrative of both classical motion and results for accelerated wave packets. Over the first cycle, when the packet is not colliding with the wall, the spread in momentum remains constant, as expected from Eqn. (13), while it increases dramatically during the collision time, just as with the ‘bouncing wavepacket’ in Ref. [5]. After each bounce, however, the spread in momentum has grown slightly so that Δp_t increases in a quasi-stepwise manner between collisions, with flat plateaus between each impulsive ‘spike’.

We now turn our attention to the long-term behavior of these solutions and plot in Fig. 5 the same quantities, $\langle z \rangle_t$, $\langle p \rangle_t$, and $|A(t)|^2$, as in Fig. 3, but now over an interval

containing two expected revivals; these are indicated by the bold vertical dashed lines. We also indicate the collapse time, given by Eqn. (21), after $t = 0$ as well as one unit of collapse time around each expected revival. The reformation of the wavepacket at the revivals is clearly apparent in all three variables, as is the approach to the more constant values during the collapsed phases.

The horizontal dashed lines around which the quantum mechanical expectation values cluster during the collapsed phases are given by the average values derived from purely classical probability densities. Using standard arguments about how much time a particle spends in a small interval of position, we can find the normalized position-space classical probability as

$$P_{CL}(z) = \frac{1}{2\sqrt{A(A-z)}} \quad \text{for } 0 < z < A \quad (23)$$

and which vanishes for all other values of z . The classical turning point, A , is given by $E = FA$, and we naturally associate A with the initial position z_0 in our quantum analysis. With this identification, the classical average values are

$$\begin{aligned} \langle z \rangle &= \int_0^{z_0} z P_{CL}(z) dz = \frac{2}{3}z_0 \\ \langle z^2 \rangle &= \int_0^{z_0} z^2 P_{CL}(z) dz = \frac{8}{15}z_0^2 \\ \Delta z &= \sqrt{\langle z^2 \rangle - \langle z \rangle^2} = \frac{2}{\sqrt{45}}z_0. \end{aligned} \quad (24)$$

For the momentum-space probability distribution, we note that for a constant force, the probability density is uniform over the allowed space of values, namely

$$P_{CL}(p) = \frac{1}{2p_M} \quad \text{for } -p_M < p < +p_M \quad (25)$$

and vanishing for $|p| > p_M$: in this expression we have $p_M = \sqrt{2mE} = \sqrt{2mFA} = \sqrt{2mFz_0}$. The classical averages are then given by

$$\begin{aligned}\langle p \rangle &= 0 \\ \langle p^2 \rangle &= \frac{1}{3}p_M^2 \\ \Delta p &= \sqrt{\langle p^2 \rangle - \langle p \rangle^2} = \frac{1}{\sqrt{3}}p_M.\end{aligned}\tag{26}$$

These results are known to agree well (after local averaging) with the position- and momentum-space probability densities corresponding to time-independent energy eigenstates for this type of potential [24]. We would expect that the quantum wave packet expectation values to closely match these classical results (again, after local averaging) during the collapsed phase as well, since the wave function is closer to being an incoherent sum of many such stationary states rather than the highly coherent, well-localized, quasi-periodic state close to the initial time and later revivals. The time-dependent values of $\langle z \rangle_t$ and $\langle p \rangle_t$ in Fig. 5 do collapse to just these values.

For the autocorrelation function we have no classical analog, but we can formally evaluate $|A(t)|^2$ in terms of the expansion coefficients, c_n , of the wave packet. In the limit that the various time-dependent components of the packet get out of phase, we have the expectation that during the collapsed interval

$$|A(t)|^2 = \left| \sum_{n=1}^{\infty} |c_n|^2 e^{iE_n t/\hbar} \right|^2 = \sum_{n,m=1} |c_n|^2 |c_m|^2 e^{i(E_n - E_m)t/\hbar} \longrightarrow \sum_{n=1} |c_n|^4 \tag{27}$$

as the ‘off-diagonal’ terms tend to cancel as they have lost the phase coherence built into the initial state. This limiting value, calculated using the numerically determined c_n , is plotted in Fig. 5 (as the bold horizontal dashed line) and compares well to the locally averaged value of $|A(t)|^2$ during much of the collapsed period.

In Fig. 6, we plot the position- and momentum-spreads, as in Fig. 4, but once again over the longer time interval, and superimpose the classical (constant) expectation

values for Δz and Δp as bold horizontal dashed lines. In both plots, the quantum wave packet expectation values and uncertainties cluster appropriately around the classical results of Eqns. (24) and (26) during the collapsed phase as expected.

Finally, one of the most interesting results of Ref. [10] is that the wave packet revivals happen in such a way that the probability densities are almost completely out of phase with the classical motion. In order to visualize this effect in the expectation value approach followed here, we plot again the same quantities as in Fig. 3, namely $\langle z \rangle_t$, $\langle p \rangle_t$, and $|A(t)|^2$, also over a time interval corresponding to 8 classical periods, but now centered around the expected revival time. In each case we indeed see that the quantum expectation values (solid) are approximately half a cycle out of phase with the corresponding classical trajectory values (dashed) and that the autocorrelation function is peaked at regular intervals, but offset from integral multiples of the classical period by roughly $T_{cl}/2$.

In conclusion, we have reexamined the interesting problem of quasi-Gaussian wave packets for the quantum bouncer, focusing on the numerical calculation and visualization of the results through the expectation values and uncertainties of position and momentum. We have focused on a single classical period to illustrate the important similarities and significant differences between this case and well-studied periodic wave packet solutions to other familiar problems such as the harmonic oscillator and infinite well as well as to the closed-form solutions for the constant acceleration case in Eqns. (15) and (16). We have also examined these quantities over the first few periods, well before the collapsed phase and compared them to classical trajectory expectations. Finally, we have confirmed, numerically and through visualization, that the quantum expectation values approach (in a locally averaged sense) the purely classical results from the time-independent probability distributions in Eqns. (24) and (26) during the

collapsed phase as well as illustrating the expected phase relationships between the classical trajectories and quantum expectation values near the revivals.

Acknowledgments

The work of MAD was supported, in part, by the Commonwealth College of The Pennsylvania State University under a Research Development Grant (RDG); the work of RR was supported, in part, by NSF grant DUE-9950702.

References

- [1] B. Thaller, *Visual Quantum Mechanics: Selected Topics with Computer-Generated Animations of Quantum-Mechanical Phenomena* (Springer-Verlag, New York, 2000).
- [2] S. Brandt and S. Dahmen, *The Picture Book of Quantum Mechanics*, Third Edition (Springer-Verlag, New York, 2001).
- [3] J. Bayfield, *Quantum Evolution: An Introduction to Time-Dependent Quantum Mechanics* (Wiley, New York, 1999).
- [4] J. R. Hiller, I. D. Johnston, and D. F. Styer, *Quantum Mechanics Simulations: The Consortium for Upper-Level Physics Software*, (Wiley, New York, 1995).
- [5] A rather comprehensive list of references to discussions of wave packet propagation in many model quantum mechanical systems, both for scattering and for bound states, in the pedagogical literature is contained in M. Doncheski and R. W. Robinett, “Anatomy of a quantum ‘bounce’”, *Eur. J. Phys.* **20**, 29-37 (1999).
- [6] R. Bluhm, V. A. Kostelecký, and J. A. Porter, “The evolution and revival structure of localized wave packets”, *Am. J. Phys.* **64**, 944-953 (1996).
- [7] D. L. Aronstein and C. R. Stroud Jr., “Fractional wave-function revivals in the infinite square well”, *Phys. Rev. A* **55**, 4526-4537 (1997).
- [8] P. Stifter, E. W. Lamb Jr, and W. P. Schleich, “The particle in a box revisited” in *Frontiers of Quantum Optics and Laser Physics, Proceedings of the International Conference on Quantum Optics and Laser Physics* (Springer, Singapore, 1997), pp. 236-246.

- [9] R. W. Robinett, “Visualizing the collapse and revival of wave packets in the infinite square well using expectation values”, *Am. J. Phys.* **68**, 410-420 (2000).
- [10] J. Gea-Banacloche, “A quantum bouncing ball”, *Am. J. Phys.* **67**, 776-782 (1999).
- [11] O. Valee, “Comment on “A quantum bouncing ball,” by Julio Gea-Banacloche”, *Am. J. Phys.* **68** 672-673 (2000). This Comment describes how some of the mathematical results obtained numerically in Ref. [10] can be derived more rigorously.
- [12] For many references to discussions of time-independent solutions of the quantum bouncer problem, see Ref. [10].
- [13] D. S. Saxon, *Elementary Quantum Mechanics* (McGraw-Hill, New York, 1968), pp. 144-147.
- [14] D. F. Styer, “The motion of wave packets through their expectation values and uncertainties“, *Am. J. Phys.* **58**, 742-744 (1989).
- [15] A. S. de Castro and N. C. da Cruz, “A pulsating Gaussian wave packet”, *Eur. J. Phys.* **20**, L19-L20 (1999).
- [16] J. Arnaud, “Pulsating Gaussian wavepackets and complex trajectories”, *Eur. J. Phys.* **21**, L15-L16 (2000).
- [17] M. Nauenberg, “Autocorrelation function and quantum recurrence of wavepackets”, *J. Phys. B. At. Mol. Opt. Phys.* **23**, L385-390 (1990).
- [18] R. W. Robinett, *Quantum Mechanics: Classical Results, Modern Systems, and Visualized Examples*, (Oxford University Press, New York, 1997), p. 102-103.
- [19] R. W. Robinett, “Quantum mechanical time-development operator for the uniformly accelerated particle”, *Am. J. Phys* **64**, 803-808 (1996).

- [20] B. R. Holstein, “The linear potential propagator”, Am. J. Phys **65**, 414-418 (1997)
- [21] G. Vandegrift, “Accelerating wave packet solution to Schrödingers equation”, Am. J. Phys **68**, 576-577 (2000).
- [22] R. W. Robinett, “Wave packet revivals and quasirevivals in one-dimensional power law potentials”, J. Math. Phys **41**, 1801-1813 (2000).
- [23] M. Andrews, “Wave packets bouncing off walls”, Am. J. Phys. **66**, 252-254 (1998).
- [24] R. W. Robinett, “Quantum and classical probability distributions for position and momentum”, Am. J. Phys. **63**, 823-832 (1995).

Figure Captions

Fig. 1. Gaussian wave packet solutions for the quantum bouncer in position-space ($|\psi(z, t)|^2$ versus z , left) and momentum-space ($|\phi(p, t)|^2$ versus p , right) for various times during the first classical period. The solid curves represent the time-dependent expectation values of position ($\langle z \rangle_t$, left) and momentum ($\langle p \rangle_t$, right) for these solutions. The similar dashed curves are the classical trajectories, $z(t)$ (left) and $p(t)$ (right), superimposed. The wave packet parameters in Eqn. (19) are used. For the momentum-space figure, the vertical dotted lines represent the values $p = 0$ and the classical extremal values of momentum, $\pm p_M = \pm\sqrt{2mFz_0}$.

Fig. 2. Plots of the classical momentum versus time, $p(t)$ versus t , for objects released from a height H with initial momenta given by $p(0) = 0$ (solid), $p(0) = \pm\Delta p$ (dotted), and $p(0) = \pm 2\Delta p$ (dashed). After one classical period, the distribution of momentum values is asymmetric about $p = 0$, in just the same way as the $|\phi(p, t)|^2$ plot in Fig. 1; compare the momentum values defined by the $t = 0$, $(+2\Delta p, -2\Delta p)$ 'band' to the corresponding values at $t = T_{cl}$.

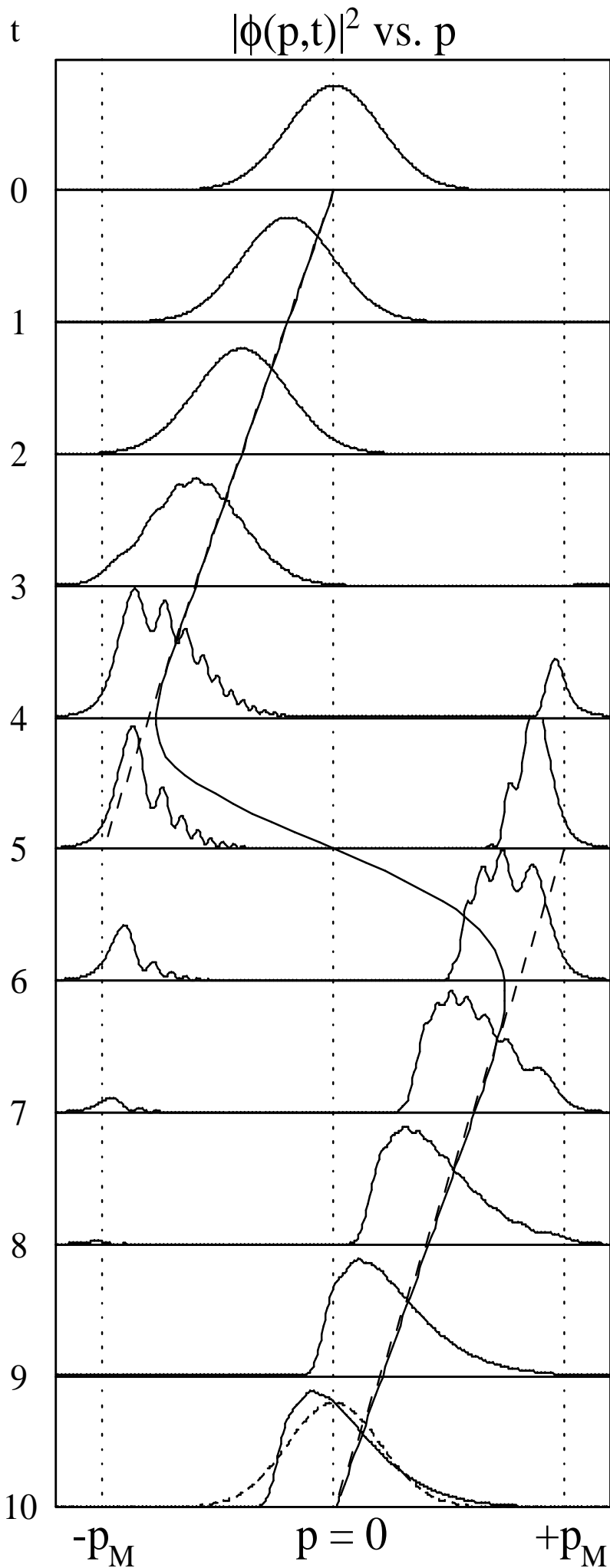
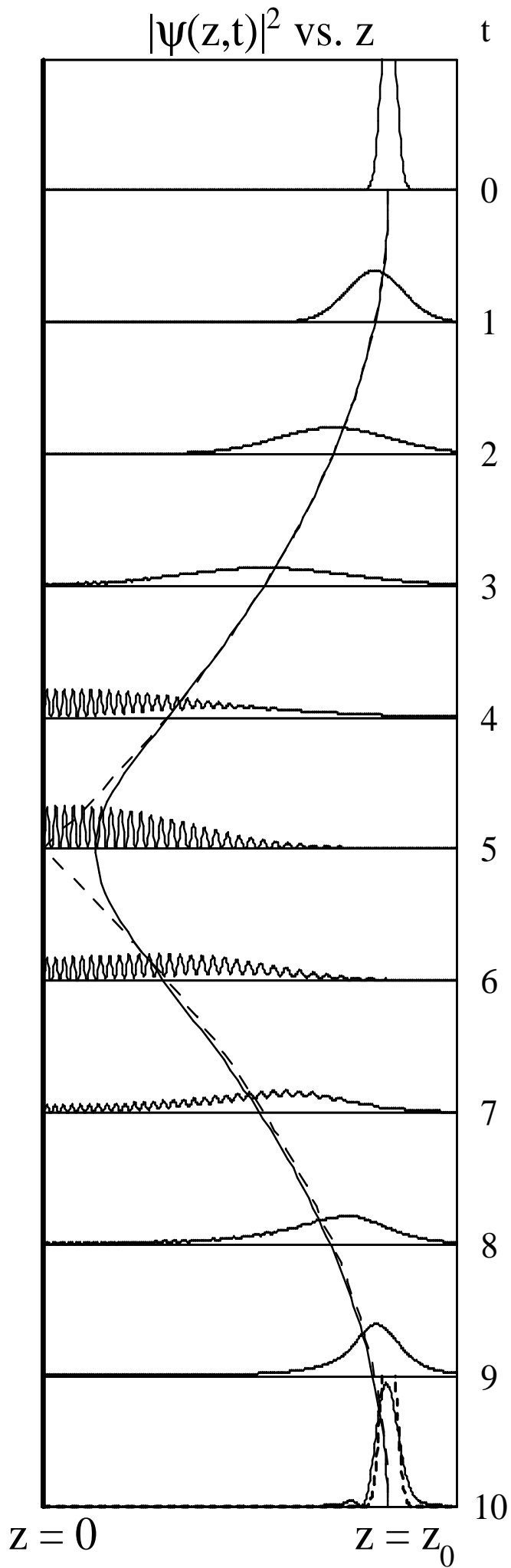
Fig. 3. The solid curves represent the expectation values of position ($\langle z \rangle_t$, top) and momentum ($\langle p \rangle_t$, middle) and the autocorrelation function ($|A(t)|^2$, bottom) versus time for the first eight classical periods of motion for the bouncing wave packet. The wave packet parameters in Eqn. (19) are used. The dashed lines are the classical trajectories for comparison. The horizontal line in the top figure corresponds to the average value of position over one classical period, namely $\langle z \rangle = 2z_0/3$, from Eqn. (24).

Fig. 4. Same as Fig. 3 except that the time-dependent values of the uncertainty in position (Δz_t , top) and momentum (Δp_t , bottom) are shown over the first eight periods. The dashed curves in the top picture correspond to the spreading (anti-spreading) of a Gaussian wave packet as it 'slides' downhill (uphill) as in Eqn. (22); these expressions agree well with the observed values of Δz_t during the first period, except during those times when the packet is 'bouncing' against the infinite wall at $z = 0$, near $T_{cl}/2 = 5$. The dashed line in the Δp_t figure (bottom) indicates the classical spread in momentum defined in Eqn. (26), $\Delta p = p_M/\sqrt{3}$.

Fig. 5. Same as Fig. 3, but now over a longer time scale, containing two revivals. The expected locations of the revivals, according to Eqn. (17), are shown as vertical dashed lines, and times within one collapse time, T_{coll} , of the initial time and these two revival times are also shown as vertical dotted lines. The classical average values of position and momentum ($\langle z \rangle = 2z_0/3$ and $\langle p \rangle = 0$) from Eqns. (24) and (26) are shown as bold horizontal dashed lines, as is the expected value of the autocorrelation function during the collapsed phase, $|A(t)|^2 = \sum_n |c_n|^4$, from Eqn. (27), using the numerically determined values of the c_n .

Fig. 6. Same as Fig. 3, except for the long term values of Δz_t and Δp_t . The classical average values of these quantities ($\Delta z = 2z_0/\sqrt{45}$ and $\Delta p = p_M/\sqrt{3}$) from Eqns. (24) and (26) are shown as bold horizontal dashed lines.

Fig. 7. Same as Fig. 3, except for an eight classical period time window around the first revival which is indicated by the bold vertical dashed line. Note how the quantum mechanical averages, $\langle z \rangle_t$ and $\langle p \rangle_t$ (solid curves), are out of phase with the classical trajectory values (dashed curves). In the bottom figure, the dashed curve corresponds to the time-development of the auto-correlation function, $|A(t)|^2$, over the first eight periods of the motion, for comparison.



$p(t)$ vs. t

